



Fusion Methods and Multi-classifiers to Improve Land Cover Estimation Using Remote Sensing Analysis

Hayder Dibs · Hashim Ali Hasab · Ammar Shaker Mahmoud · Nadhir Al-Ansari 

Received: 28 February 2021 / Accepted: 27 May 2021 / Published online: 5 June 2021
© The Author(s) 2021

Abstract Adopting a low spatial resolution remote sensing imagery to get an accurate estimation of Land Use Land Cover is a difficult task to perform. Image fusion plays a big role to map the Land Use Land Cover. Therefore, This study aims to find out a refining method for the Land Use Land Cover estimating using these steps; (1) applying a three pan-sharpening fusion approaches to combine panchromatic imagery that has high spatial resolution with multispectral imagery that has low spatial resolution, (2) employing five pixel-based classifier approaches on multispectral imagery and fused images; artificial neural net, support vector machine, parallelepiped, Mahalanobis distance and spectral angle mapper, (3) make a statistical comparison between image classification results. The

Landsat-8 image was adopted for this research. There are twenty Land Use Land Cover thematic maps were generated in this study. A suitable and reliable Land Use Land Cover method was presented based on the most accurate results. The results validation was performed by adopting a confusion matrix method. A comparison made between the images classification results of multispectral imagery and all fused images levels. It proved the Land Use Land Cover map produced by Gram–Schmidt Pan-sharpening and classified by support vector machine method has the most accurate result among all other multispectral imagery and fused images that classified by the other classifiers, it has an overall accuracy about (99.85%) and a kappa coefficient of about (0.98). However, the

H. Dibs
Water Resources Engineering Faculty, Hydraulic Structures Engineering Department, Al-Qasim Green University, Babel, Iraq
e-mail: Dr.hayderdibs@wrec.uoqasim.edu.iq;
haiderdibs@gmail.com

H. Dibs
Iraqi Environment Upgrading and Development Organization, Karbala, Iraq

H. A. Hasab
Architectural Design and Decoration Department, Al-Furat Al-Awsat Technical University, Technical Institute of Najaf, Najaf, Iraq
e-mail: hasab.hashim1979@gmail.com;
hashim@atu.edu.iq

A. S. Mahmoud
Civil Engineering Department, College of Engineering, University of Babylon, Babylon, Iraq
e-mail: ammar.shaker.eng@uobabylon.edu.iq

N. Al-Ansari (✉)
Department of Civil Environmental and Natural Resources Engineering, Lulea University of Technology, 971 87 Lulea, Sweden
e-mail: nadhir.alansari@ltu.se

spectral angle mapper algorithm has the lowest accuracy compared to all other adopted methods, with overall accuracy of 53.41% and the kappa coefficient of about 0.48. The proposed procedure is useful in the industry and academic side for estimating purposes. In addition, it is also a good tool for analysts and researchers, who could interest to extend the technique to employ different datasets and regions.

Keywords Image fusion · Intensity–hue–saturation sharpening · Image classification · Land use and land cover · Gram–Schmidt spectral sharpening · Brovey spectral sharpening

1 Introduction

An accurate thematic map of Land Use Land Cover (LULC) plays a big role in different remote sensing applications such as; change detection, environment managing and monitoring, LULC detection, hazard prediction, urban area expansion, forest monitoring and other (Sang et al. 2014; Khatami et al. 2016; Dibs et al. 2017; Zhang et al. 2018; Karar et al. 2020). Image fusion plays a big role to refine and improve the estimation of LULC. In other hand, remote sensing is a powerful tool and very useful for mapping the LULC from using a suitable satellite images with a good selecting of classification method. However, image classification approaches consider as the best method to monitor, manage and estimate the LULC (Dibs 2013; Sang et al. 2014). To perform classification, it needs to involve different stages such as selection training and testing samples, atmospheric correction, radiometric correction, geometric correction, objects extraction, classifier method selection, post-classification process, and performing results validation (Singh et al. 2014; Dixon et al. 2015; Hayder et al. 2018; Dibs 2018).

The Selection of a reliable classifier technique is very critical to obtain an accurate LULC map (Dixon et al. 2015; Li et al. 2017). For LULC estimating there are large numbers of techniques and methodologies to apply, some of these classifiers under pixel-based and other under object-based, these algorithms such as the artificial neural net (ANN), support vector machine (SVM), parallelepiped (PP), Mahalanobis distance (Mah) and spectral angle mapper (SAM), Decision

Trees (DT) as discussed by (Chasmer et al. 2014; Elatawneh et al. 2014; Iounousse et al. 2015; Hayder et al. 2015; Löw et al. 2015; Zhang et al. 2018). Additionally, many improved techniques have been applied to improve LULC mapping such as the image pan-sharpening technique (Ghosh et al. 2014; Cavour et al. 2019). These approaches can be divided into many categories; component substitution techniques, multi-resolution dataset analysis (Li et al. 2017). Firstly, there are two basic types of fusion pan-sharpening methods; regarding color, statistical and numerical algorithms (Ma et al. 2019). The most commonly adopted method is regarding to component substitution. Intensity hue saturation spectral sharpening (IHS) method is one of the commonly employed methods of the IHS group (Li et al. 2017). IHS works based on color space transformation (Paidamwoyo et al. 2020). However, the GS method is a new generation of pan-sharpening approaches of deep learning, it has been adopted widely in previous years, it relies on the applications of color transform and it converts low-resolution multi-spectral band to a new color system that differences in both spatial and spectral information and details (Paidamwoyo et al. 2020). The principal component analysis (PCA) method is another one to use, and it works based on a statistical method, therefore, PCA is included under the group of statistical methods (Cavour et al. 2019). The Brovey method is a multiplicative approach, it is modified by normalization of the results (Elatawneh et al. 2014). Many studies discuss imagery pan-sharpening between panchromatic (PAN) and multi-spectral (MS) images (Sang et al. 2014; Khatami et al. 2016; Li et al. 2018; Hayder et al. 2020). The spatial resolution will enhance when, replacing the PAN imagery that has high-spatial resolution by the MS image that has high-spectral resolution without saving all spectral information (Li et al. 2018; Azarang and Kehtarnavaz 2020). The purposes behind using imagery pan-sharpening method are; (1) upsurging of spatial resolution, (2) advancing of geometric accurateness, (3) improving topography presentation, (4) refining of classification precision (Ma et al. 2019).

There are several pan-sharpening methods that have been adopted using remotely sensed data throughout the world. However, some key unanswered questions: (a) does incorporate PAN imagery will support the LULC mapping? (b) What is the best pansharpening fusion method between the Landsat

MS and PAN data? (c) What is the best algorithm to classify to produce LULC Landsat data? To address all these questions, the current research focuses on investigating the pansharpening of PAN and MS Landsat images and examine it with different pixel-based classification approaches to propose an improved procedure for estimating LULC. The layout of this article will start with the used materials and methods section, and then go through collecting the truth dataset, performing an image noise removal (geometric and radiometric noise) for all images. The next step will be conducting the image fusion levels. Then, apply different classification methods on the Multi-spectral and fused images. The Discussion section will show the discuss in deep all the outcomes of these processing and analysis to get the most accurate methodology to map the LULC.

The outcomes of this study will help to provide a big contribution to industry and academic fields. Analysts and researchers can improve, develop and extend the present method to work and apply on different dataset sources and regions.

2 Materials and Methods

For this research different processing, analyzing and integrating methods were adopted to find an appropriate procedure for generating the LULC map. In this study, start with downloading the datasets from Landsat-8 satellite (PAN and MS) imagery in 20/2/2018, then a noise removed is starting in order to remove and reduce images radiometric and geometric errors. The next step, it was satellite images resampling using bilinear approach. Then the Landsat-8 (PAN and MS) images become ready for further processing and analysis stages. This research has two different procedures to estimate the LULC. Firstly, the Landsat-8 MS images classified with a five pixel-based classifier approaches (PP, ANN, SVM, SAM, and Mah), with selecting the same training and testing sites to conduct each classification algorithm and to give a good result reflections when perform a statistical comparison in the next step of this research. Secondly, the Landsat-8 PAN and MS satellite images were integrating together with a three different image fusion levels; Gram-Schmidt Pan-sharpening (GS), IHS spectral sharpening and Brovey pan-sharpening method. Each level of images fusion go through the

five pixel-based classification methods with using the same collected training and testing sites of the PAN and MS satellite images to examine which methodology will provide the most accurate result to produce LULC map. As indicated above the MS and fused satellite images will be classified into twenty times for the purpose of this study. After that, a confusion matrix will apply on the results of the twenty classified images to validate their accuracy. Then, the outcomes of all the previous stages will examine from making a statistical comparison between them. Figure 1 indicates the adopted method for this study.

2.1 Study Area Description

In this research, Baghdad city was selected as the study area. Baghdad city is a very famous city in Iraq and the world. It considers as the second-largest city in the Arab world after Cairo city in the term of population. It has a location along the Tigris River. In the eighth century, Baghdad city has a golden history, it became the Abbasid caliphate capital city that time. Baghdad has a significant in both commercial and cultural fields in the Arab world. It has a population of about 6,719,500 person regarding to the estimate of 2018, this population value makes this city as one of the biggest cities in there public of Iraq (Dibs 2018). It is located in $44^{\circ} 27' 54.37''$ Easting and $33^{\circ} 23' 03.98''$ Northing. The area of Baghdad city is around 204.2 km^2 and its altitude ranges in between (32–38) m above the mean sea level (MSL) (Hayder et al. 2020). Figure 2 indicates the location of an interesting area of this study.

2.2 Satellite Images and Truth Dataset

The satellite imagery was obtained from the Landsat-8 sensor. This sensor is launched into space on 11/2/2013 (Dibs 2018). The Landsat sensor has carried two different sensors, the operational land imager (OLI) and Thermal Infrared Sensor (TIRS). Landsat satellite data has (11) bands, some of them have a spatial resolution of about 30 m for each band of (1 to 7 & 9). However, the PAN channel (8 band), it has a spatial resolution of about 15 m. In addition, the thermal bands (10 and 11) have a spatial resolution of 100 m. Table 1 describes the specifications of Landsat sensor bands. The dataset for this research was freely downloaded from the Glovis website (<https://glovis>).

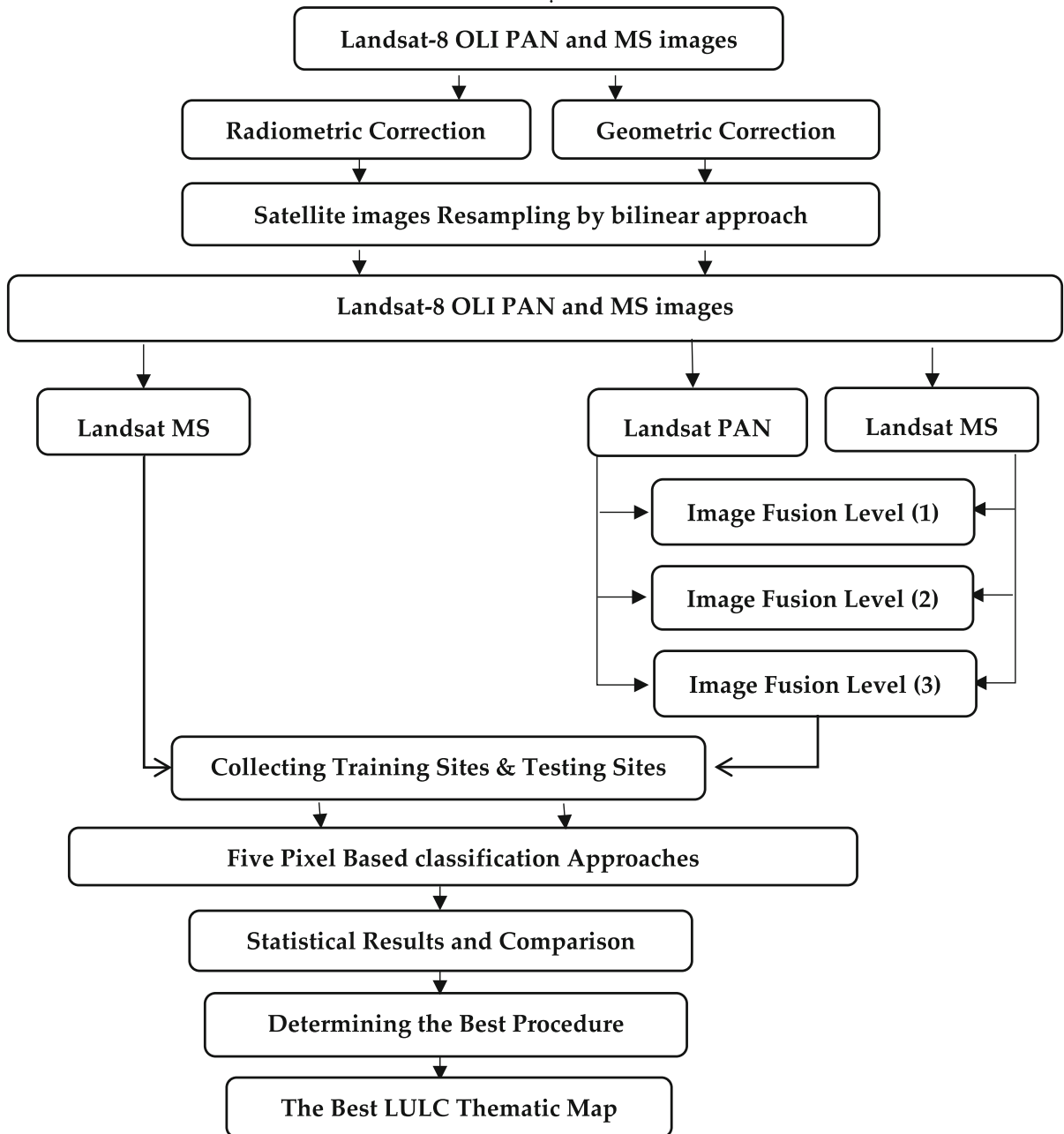


Fig. 1 Flowchart of adopted method

[usgs.gov/app](https://www.usgs.gov/app)) with path = 168 and row = 37. The satellite image was captured on 20/2/2018 and it has level processing 1 T standard geometric correction but without radiometric correction, UTM projection with zone 38 N, and datum a WGS 84. The processed image has no cloud.

The ground truth data must be observed to apply the pixel-based classifications. The truth data usually collect from using different methods such as collecting GPS references in fieldwork and/or higher resolution remotely sensed imagery (Lu et al. 2011; Hayder and Suhad 2019; Hayder et al. 2020). However, in this research, the authors used Google Earth Pro to collect

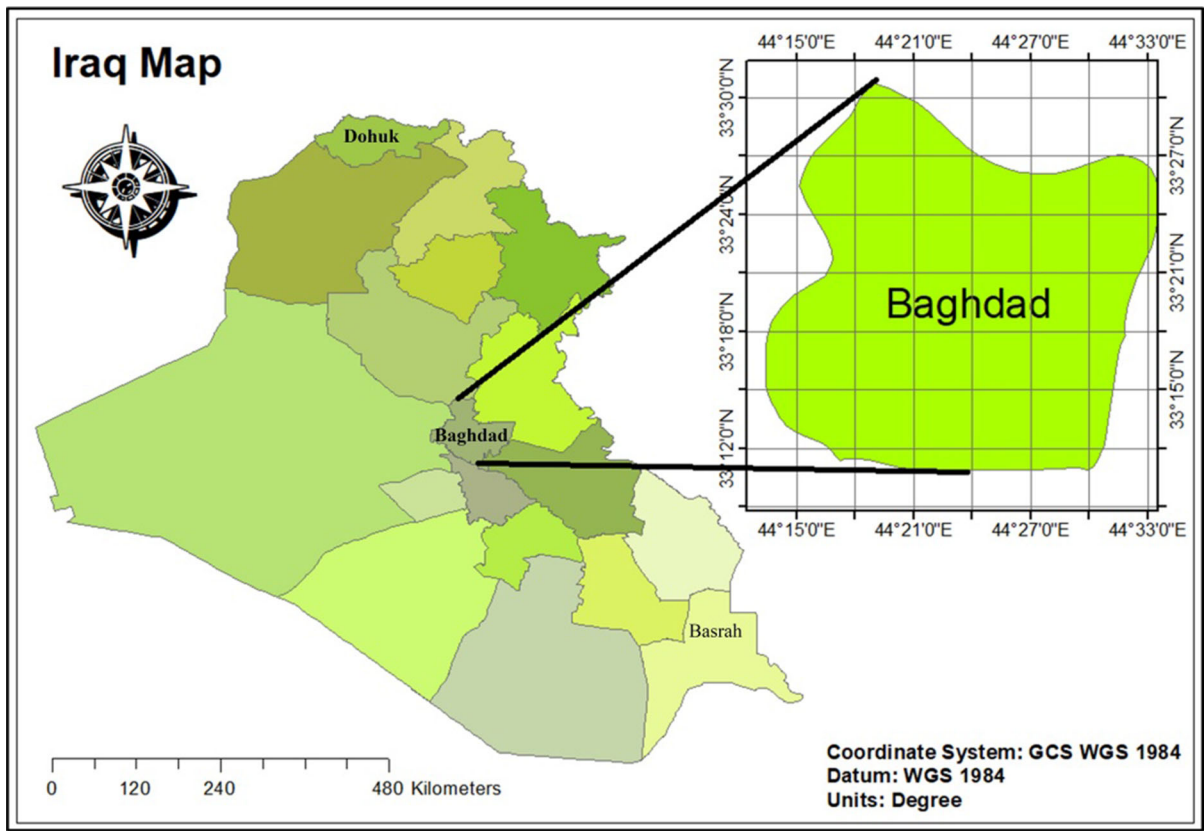


Fig. 2 Location of the study area, Baghdad city, IRAQ

Table 1 Describes the specifications of Landsat bands

| Bands | Spectral wavelength range (μm) | Spatial resolution (m) |
|------------|---|------------------------|
| Channel 1 | 00.44–0.45 | 30 |
| Channel 2 | 00.45–0.51 | |
| Channel 3 | 00.53–0.59 | |
| Channel 4 | 00.64–0.67 | |
| Channel 5 | 00.85–0.88 | |
| Channel 6 | 01.57–1.65 | |
| Channel 7 | 02.11–2.29 | |
| Channel 8 | 00.50–0.68 | 15 |
| Channel 9 | 01.36–1.38 | 30 |
| Channel 10 | 10.60–11.19 | 100 |
| Channel 11 | 11.50–12.51 | 100 |

the training and testing samples in the image by visual interpretation process for each class. The Google Earth Pro image has a very high spatial resolution, and that will help to discover the located features in the study area (Hayder et al. 2020). For this study, five classes were selected to be used in estimating of LULC map,

and they are; urban area, water body, soil area, roads and vegetation, respectively. Selecting these five classes was made based on the regular features that distribute in the study area as indicate in Fig. 3. However, urban area defines all build-up areas such as building areas and/or housing area or any other kind of

buildings (commercial, education, plaza and so on). In other side, water body class defines all water bodies located in the research area such as (rivers, marshes, and lake) and soil class represents all the barren lands area. However, the roads class represents the main roads located in the Baghdad city that covered by asphalt layer. The last class was the vegetation class, and it represents evergreen lands and the area that covered with vegetation, whether natural or cultivated by humans. Randomly training and testing sites procedure were adopted for all the five class. The training and testing sites were equally distributed overall in the image of the research area to ensure get an accurate classification outcome. For every single class, there are more than 250 pixels were collected. Figure 3 indicates the ground truth datasets that collected to involve in image classification processes.

2.3 Image Noise Removal

The geometric correction (GC) for any satellite images is required before performing any processing and

analyzing on satellite images (Zhang et al. 2018; Hayder and Suhad 2019; Aysar et al. 2020). A good selection of ground control points (GCPs) location should be done (Hayder and Suhad 2019). In this study, the geometric correction of Landsat MS and PAN images was performed using ten GCPs, which regularly distributed throughout the image portions. These GCPs were collected using the Google Earth image as mention in Sect. 2.2. The first polynomial transformation and the nearest neighbor were adopted to obtain a root mean square error (RMSE), and it was about 1.32 pixels. The next correction for Landsat images was performed a radiometric correction. It is an essential algorithm for image preprocessing to remove the effects of sun illumination (Bello and Parviz 2013; Sang et al. 2014; Hayder and Suhad 2019; Hashim et al. 2020a, b; Aysar et al. 2020). The Dark Object Subtraction (DOS) was adopted to remove the radiance errors of MS and Pan. Figure 4a, b indicates the corrected MS and PAN images after removing all kind of noise.

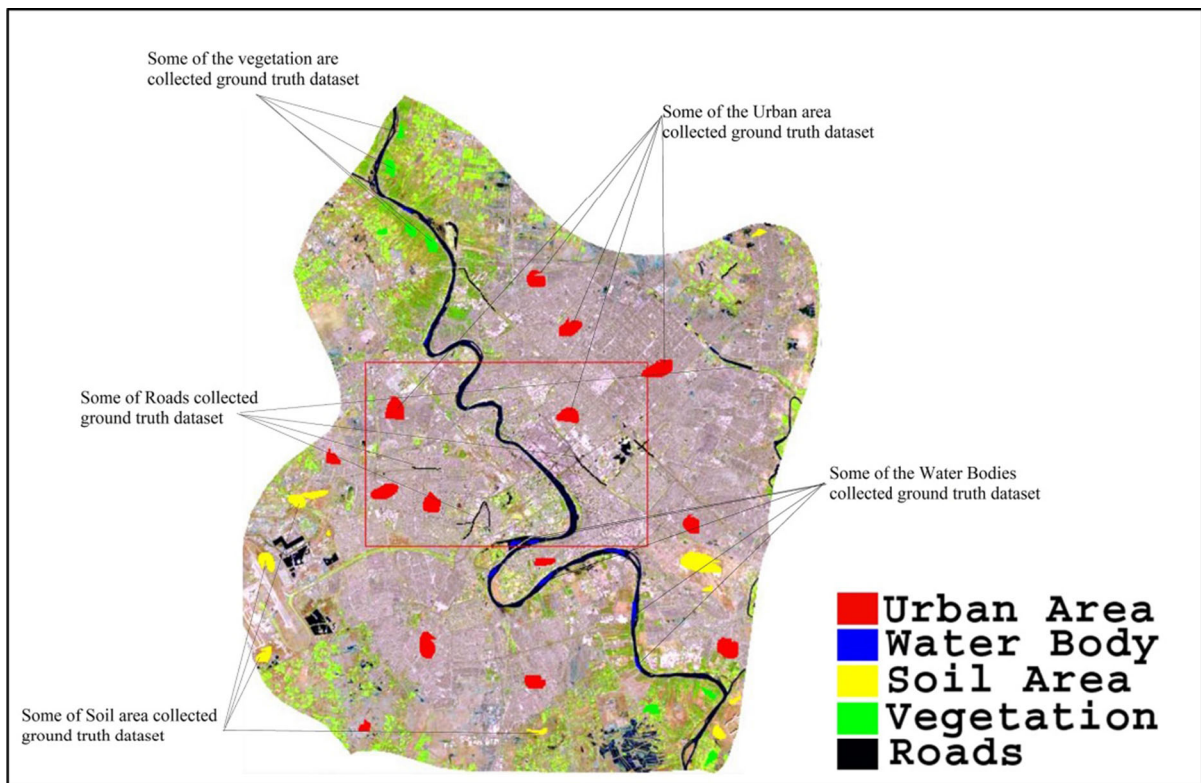


Fig. 3 The collected ground truth dataset

3 Image Fusion Levels

After conducting image layer stacking and sub-setting, the MS and PAN images will integrate together with using of a three different fusion pan-sharpening spectral methods. The first image fusion level was performed using the IHS approach. The IHS spectral sharpening method is usually adopted in imagery fusion to use the MS image complementary nature (Jain et al. 2019; Saha et al. 2019). For the spectral IHS sharpening, each of R, G and B bands of the MS data were converted to this component (Zhong et al. 2016). The PAN imagery histogram matched to the MS data intensity component (Jain et al. 2019; Hayder et al. 2020). Then, the intensity component was replaced by the PAN data. Then, the inverse transformation was conducted in order to get the MS image that has a high resolution. The pixel size of the outcome RGB imagery will have the same as the input PAN image of high-resolution. Figure 5 describes the steps of the adopted method.

The second pan-sharpening level was applied with using the Brovey method. This method adopts a mathematical combination to make integration between the high and low-resolution bands (Liu 2018) For this method, each MS band will multiply by a ratio of the band of high resolution, then divided by the MS band. The outputs of IHS processing will automatically resample the three MS bands to the PAN pixel size (Paidamwoyo et al. 2020). The result of RGB imagery will have the pixel size of the input high-resolution data (Bovolo et al. 2010). The Brovey method equation is defined below:

$$DN_{fusedMSi} = \frac{DN_{bi}}{DN_{b1} + DN_{b2} + \dots + DN_{bn}} DN_{PAN} \tag{1}$$

where (DN) represents as a particular band digital number and (bi) is the MS image particular band (Ma et al. 2019).

The third applied image fusion level was performed using Gram–Schmidt spectral sharpening (GS) algorithm. The GS sharpening method enhances the MS

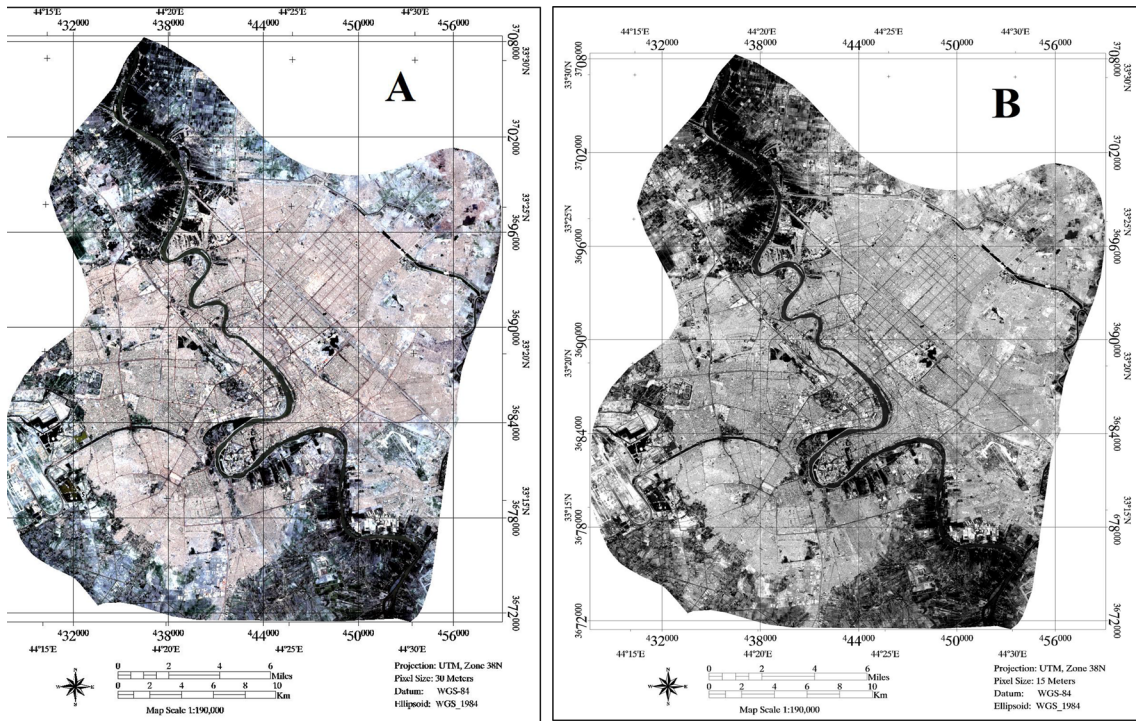


Fig. 4 a The Multi-spectral geometric corrected imagery, b the Panchromatic geometric corrected imagery

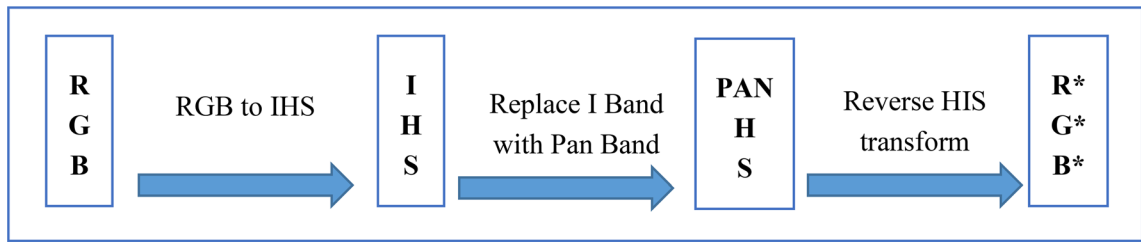


Fig. 5 IHS pan-sharpening imagery steps (Source: referenced by Liu 2018)

band's spatial resolution by integrating high and low image resolutions (Ma et al. 2019). The GS transformation conducts to the simulated high-resolution PAN band with the MS low-resolution bands. The simulated PAN high-resolution image band is adopted at the first. Then the PAN data will be replaced with the GS band (Paidamwoyo et al. 2020). The last step is inverted transformation will apply to generate the spectral sharpened MS band (Yuan et al. 2018). Figure 6a–c shows the fused images after employed the IHS, Brovey and GS spectral sharpening algorithms.

4 Classifications of Multi-spectral and Pan-sharpening Images

Many classification approaches have been adopted and applied for mapping the LULC (Yifang and Alexander 2013). However, performing image classification needs to collect the training and testing samples for

each class to guide all the processes of classifications and accuracy assessments of the output results (Rwanga and Ndambuki 2017). All the training sites will comprise to the corresponding group of the region of interests (ROIs). However, the candidates' sample groups from the same class may be spectrally (Yifang and Alexander 2013). Therefore, wide candidate pixels should be sampled (Paidamwoyo et al. 2020) There are many different supervised classifiers adopted in different remote sensing applications include PP, minimum distance, ANN, Mah, spectral information divergence, SVM, binary encoding and SAM methods (Zoleikani et al. 2017). In this study, five pixel-based classifier methods (PP, ANN, SVM, SAM, and Mah) were adopted to classify the MS data and the three fusion methods that have a good efficiency when apply on data has low spatial resolution (Taubenböck et al. 2012). The weights of the ANN method were used as uniform distribution. Values of about 0.001 and 100 were employed for

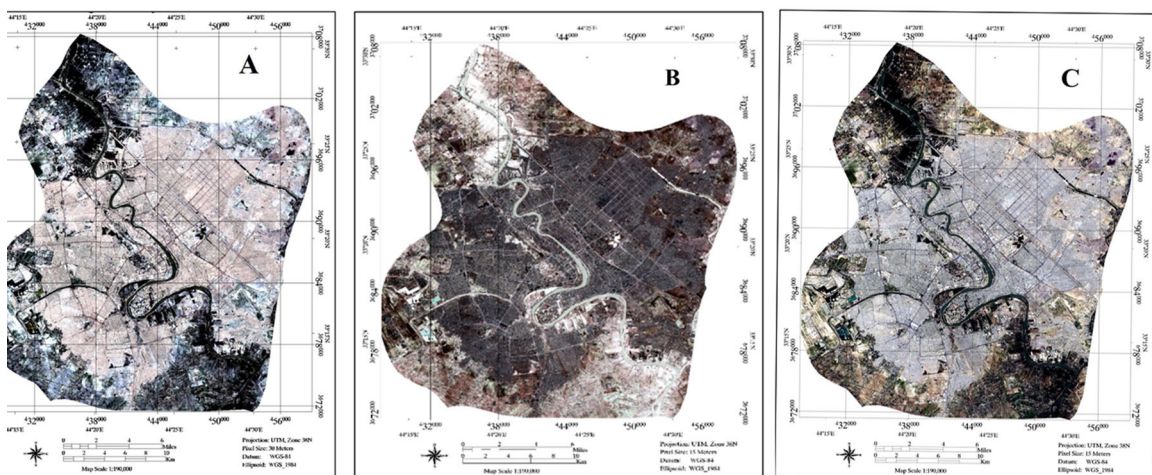


Fig. 6 Fusion algorithms: **a** IHS sharpening, **b** the Brovey sharpening, **c** the GS sharpening

learning rate for the output layer and hidden layer, respectively. So, the stopping criteria on (0.001) were fixed. However, applying the SVM approach was employed based on the default parameters, because authors for this research want to examine different classifiers, they not focus on different parameters of the SVM method. The applied SVM parameters in this research, it included of using a radial basis function as a kernel type, for gamma in kernel function. In other hand, the penalty parameter and pyramid levels were 0.167, 100.00 and 0.00, respectively. The adopted classification probability threshold value was zero. The five supervised pixel-based classification techniques were evaluated for this research using the confusion matrix (Paidamwoyo et al. 2020; Zoleikani et al. 2017). Both of overall accuracy and the kappa coefficient are widely used for quality assessment of classification results (Li et al. 2012; Pushparaj et al. 2017). In this study, these observation methods and their equations are presented below:

$$OA = \frac{\sum_{i=1}^c n_{ij}}{n} \quad (2)$$

$$\text{Kappa coefficient} = \frac{\sum_{i=1}^c n_{ij} - \sum_{i=1}^c n_i + n - i}{n^2 - \sum_{i=1}^c n_i + n + i} \quad (3)$$

where (n) is a total number of pixels, (n_{ij}) equal to the classified pixels total number, (n_i) is instances number, label (i) that has been classified in the label (j).

4.1 Landsat-8 OLI Multi-spectral image Classification

The first stage of image classification was performed by applying the supervised classifiers to classify the multispectral image of Landsat OLI by SVM, ANN, PP, Mah and SAM methods of Baghdad city and then produce the LULC thematic maps. The results of these classifiers were five thematic maps. The image processing steps were performed using the Envi 5.3 environment. The confusion matrix method was adopted to validate the classification results (Li et al. 2017, 2018; Azarang and Kehtarnavaz 2020). The validation of all classifications indicates that the SVM has the highest accuracy compared to all other adopted methods with overall accuracy (93.25) and kappa coefficient (0.92), and in both sides the statistically and visually. Figure 7 shows the thematic map of

LULC. Table 2 indicates the overall accuracies and kappa coefficients of all classifiers.

4.2 Fused Images Classifications

4.2.1 IHS Sharpening Fused Image

The IHS pan-sharpening imagery generates from integrating the MS imagery that has low-spatial-resolution and PAN imagery that has a high-spatial-resolution to refine and enhance the LULC mapping of Baghdad city, and also to obtain the highest accuracy procedure of estimating the LULC. The pan-sharpening fused image classified by employed methods of; Mah, ANN, SVM, SAM, and PP. The confusion matrix was applied in order to perform results evaluation of the five output results. A statistical comparison was made between the results of all above classifiers to get an accurate result. Statistically, the SVM method illustrates the highest overall accuracy about (98.56%) and kappa coefficient about (0.96) for IHS fused images as shown in Table 3. Figure 8 shows the results of LULC classifications of the five classifiers on HIS fused image.

4.2.2 Brovey Sharpening Fused Image Classification

Another fusion method is called the Brovey sharpening approach was adopted for this study to improve and enhance the estimating and mapping of LULC. Several types of classification algorithms were applied on the fused image by the Brovey sharpening approach; SVM, ANN, PP, Mah and SAM methods to map LULC. The confusion matrix function once again was adopted to assess the result of the five classifiers. Statistically, the SVM shows the highest OA about (98.7%) with a kappa coefficient of (0.97). Then, the obtained results were compared the classification results between the only Landsat MS image and the image fused by Brovey pan-sharpening method in order to assess the role of involving PAN data for LULC mapping and to examine if the image fusion will improve and enhance the accuracy results of LULC classification. Figure 9 and Table 4 reveal the LULC map produced by integrating PAN and MS data and classified with using several types of supervised pixel base classifiers.

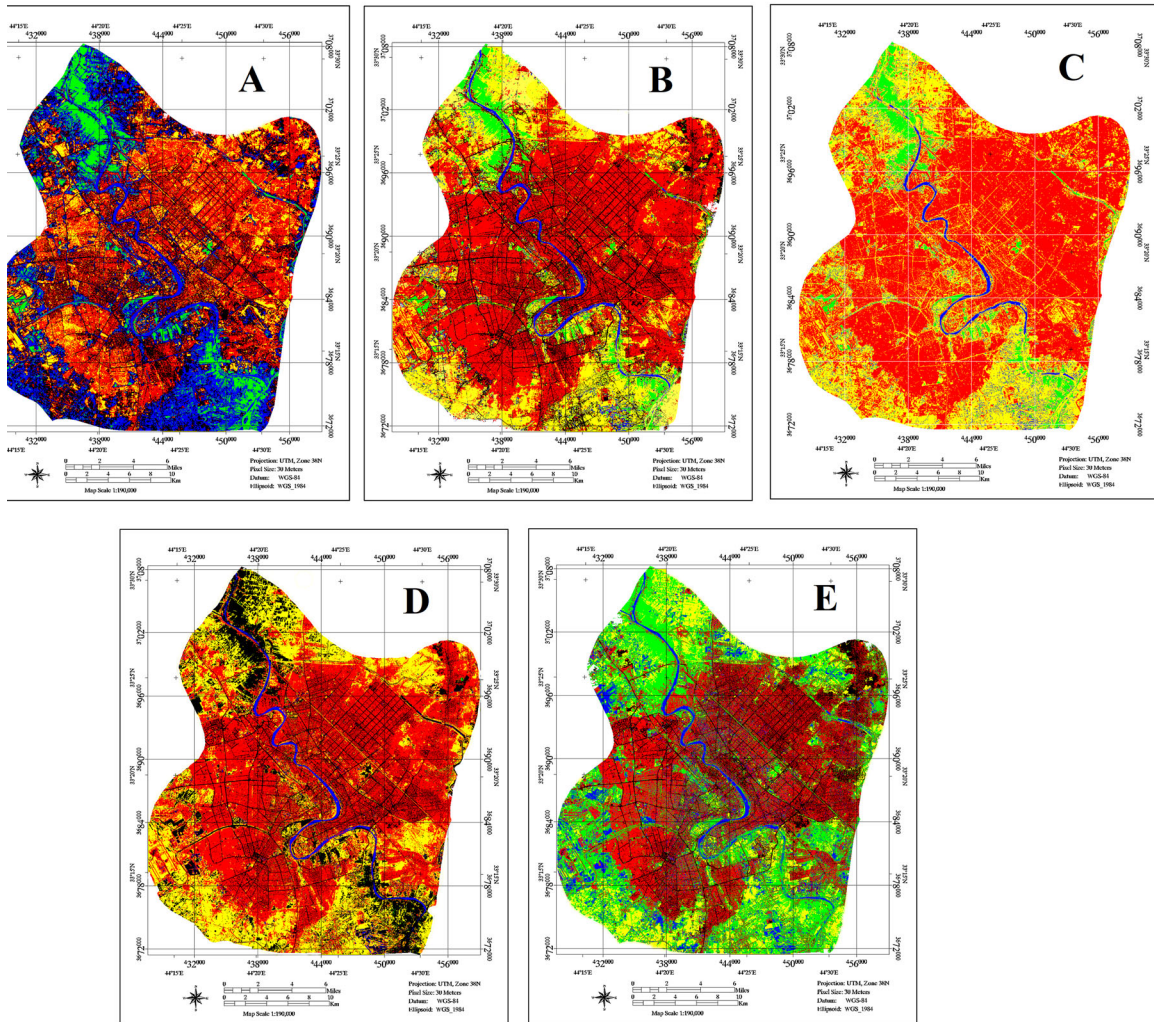


Fig. 7 The estimated LULC using Multi-spectral image classification created by applied different classification methods; **a** SVM method, **b** ANN method, **c** PP method, **d** SAM method, **e** Mah method

Table 2 The overall accuracies and kappa coefficients of all classifiers

| Type of data | Classifiers | Overall accuracy (%) | Kappa coefficient |
|------------------------|-------------|----------------------|-------------------|
| Multispectral datasets | ANN | 71.23 | 0.69 |
| | SVM | 93.25 | 0.92 |
| | PP | 76.62 | 0.70 |
| | SAM | 65.88 | 0.60 |
| | Mah | 88.15 | 0.85 |

Table 3 Overall accuracies and kappa coefficients of all classification methods

| Type of data | Classifiers | Overall accuracy (%) | Kappa coefficient |
|----------------------------|-------------|----------------------|-------------------|
| IHS sharpening fused Image | ANN | 87.23 | 0.86 |
| | SVM | 98.56 | 0.96 |
| | PP | 81.95 | 0.74 |
| | SAM | 53.41 | 0.48 |
| | Mah | 96.52 | 0.95 |

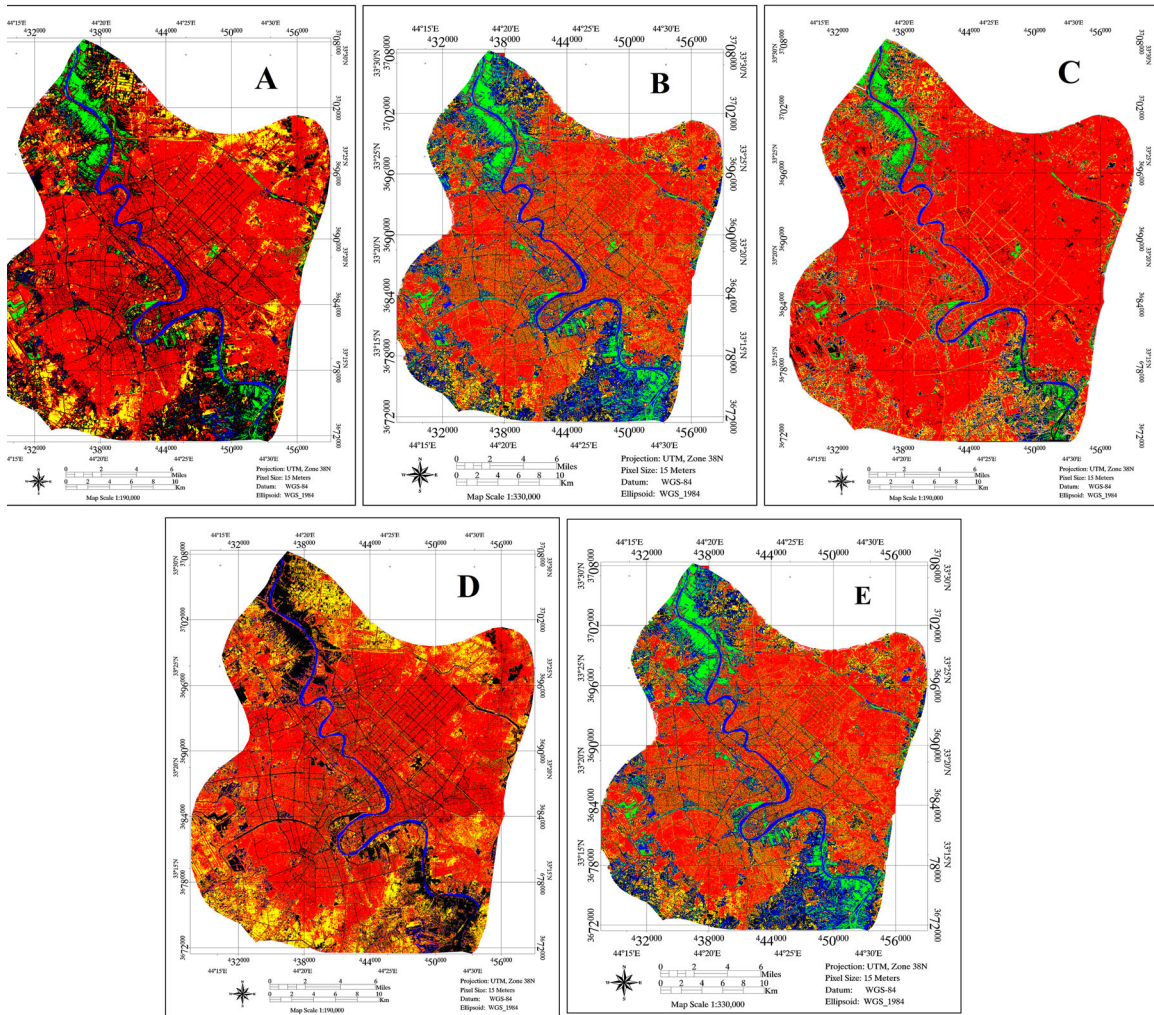


Fig. 8 LULC maps produced using different classifiers on IHS sharpening fused Image. **a** SVM, **b** ANN, **c** PP, **d** SAM, **e** Mah

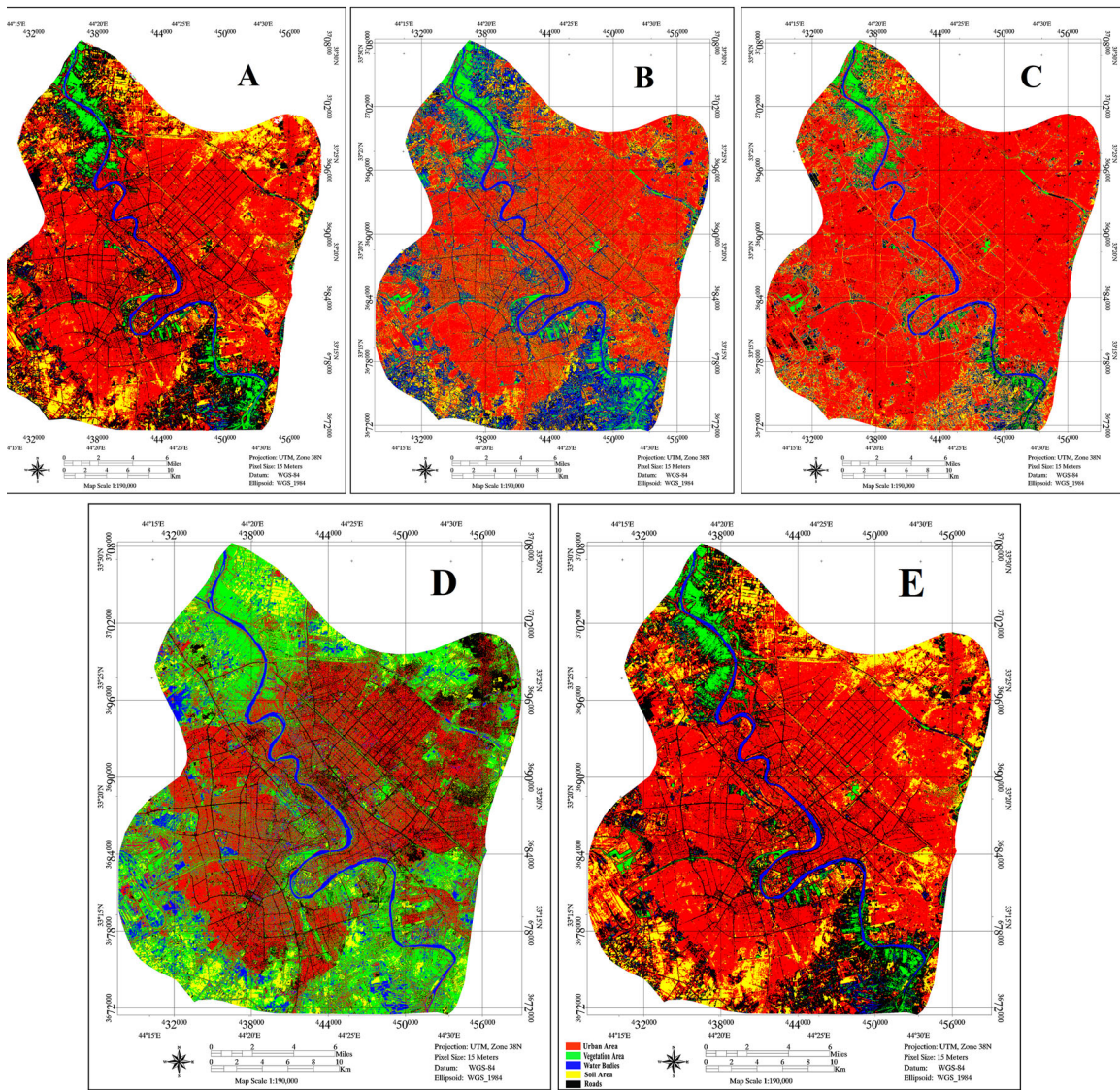


Fig. 9 LULC maps produced applies several classifiers on Brovey sharpening fused image, **a** SVM, **b** ANN, **c** PP, **d** SAM, **e** Mah

4.2.3 Gram–Schmidt Sharpening Fused Image Classification

The third spectral pan-sharpening method applied for this research was the GS sharpening algorithm. The fused image was classified by applying also the same classification approaches for previous steps: (SVM, SAM, Mah, PP and ANN) in order to estimate the LULC of Baghdad city. All the results of the fused

image classifications were evaluated using the confusion matrix technique. A statistical comparison was performed to all the results of the five classifiers in order to determine which methodology has the most accurate result. The comparison shows that using the SVM approach to classify the fused image has the highest OA about (99.85%) with a kappa coefficient of (0.98). Figures 10 and Table 5 are illustrated the integrating of the PAN and MS images. The GS

Table 4 The overall accuracies and kappa coefficients of all five classifications

| Type of data | Classifiers | Overall accuracy (%) | Kappa coefficient |
|-------------------------------|-------------|----------------------|-------------------|
| Brovey sharpening fused Image | ANN | 85.23 | 0.84 |
| | SVM | 98.70 | 0.97 |
| | PP | 83.22 | 0.76 |
| | SAM | 86.28 | 0.81 |
| | Mah | 96.99 | 0.96 |

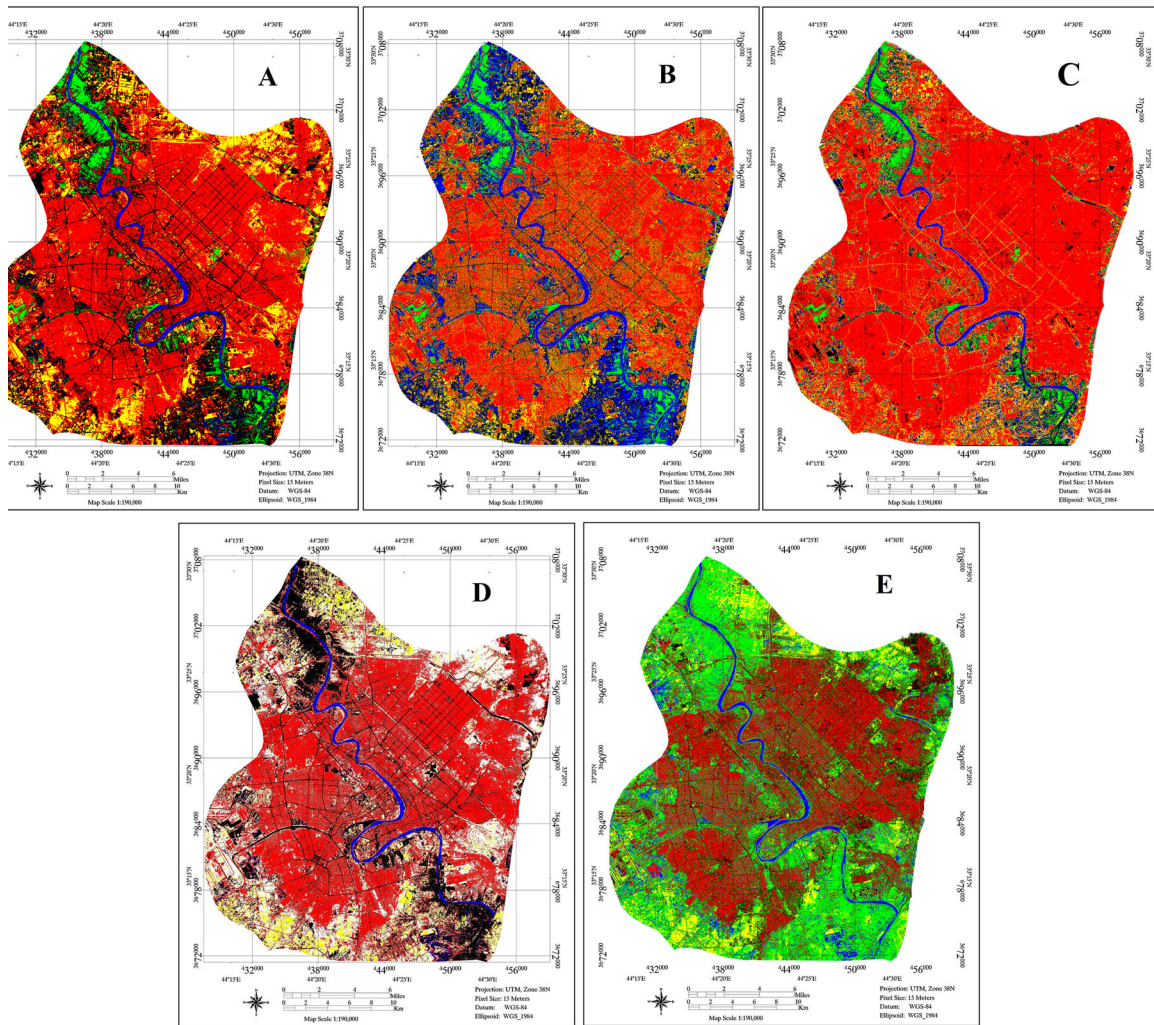


Fig. 10 LULC maps create using five classifiers onto GS spectral sharpening fused data by **a** SVM, **b** ANN, **c** PP, **d** SAM, **e** Mah

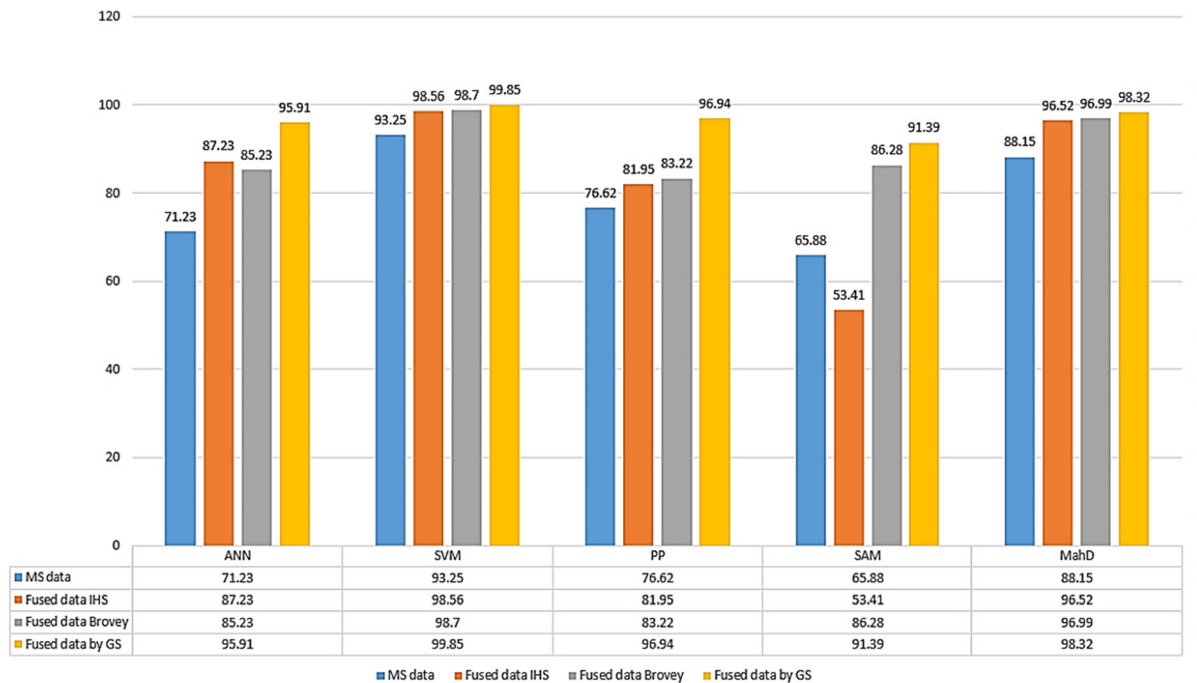
spectral pan-sharpening method with the SVM classification method reveals high improvement for image classification to generate the LULC maps.

5 Discussions

Figures 11 and 12 are representing the results of all the applied classification methods; ANN, SVM, Mah, PP

Table 5 The overall accuracies and kappa coefficients of all classifiers

| Type of data | Classifiers | Overall accuracy (%) | Kappa coefficient |
|---------------------------|-------------|----------------------|-------------------|
| GS sharpening fused image | ANN | 95.91 | 0.93 |
| | SVM | 99.85 | 0.98 |
| | PP | 96.94 | 0.90 |
| | SAM | 91.39 | 0.72 |
| | Mah | 98.32 | 0.95 |

**Fig. 11** The classification accuracies assessment of MS and fused data

and SAM in this research regarding to the level of overall accuracy and kappa coefficient that applied on the MS and the three fused pan-sharpening image by each of (IHS, Brovey and GS) sharpening algorithms. The comparison was made for this research regarding to the twenty created LULC thematic maps and the results of all the overall accuracies and kappa coefficients of all the classifiers approaches from the MS and the three image fusion levels. One of the most difficulties tasks that facing this research for images fusion was the images has different spatial resolutions. The MS image has a low-spatial resolution of about 30 m and for PAN image has a high-spatial resolution of about 15 m, and the image fusion provides superior spatial details and information (Xing et al. 2018). Different researches deal with imagery fusion between

PAN and MS images, it conducts from combining the PAN image that has features with high-frequency with the spectral information of MS image that has features with low-frequency (Azarang and Kehtarnavaz 2020). Replacing the MS image high-frequency features with the PAN image high-frequency features, will enhance the spatial resolution with loss of some spectral information (Azarang and Kehtarnavaz 2020). Therefore, for this research as indicated previously in Fig. 1. Image resampling was made by using a bilinear approach and the resampling process was performed with Envi software. So, by resampling the spatial resolution of MS image from using image fusion with PAN image, it could be obtained a good results and also enhance the LULC estimation map.

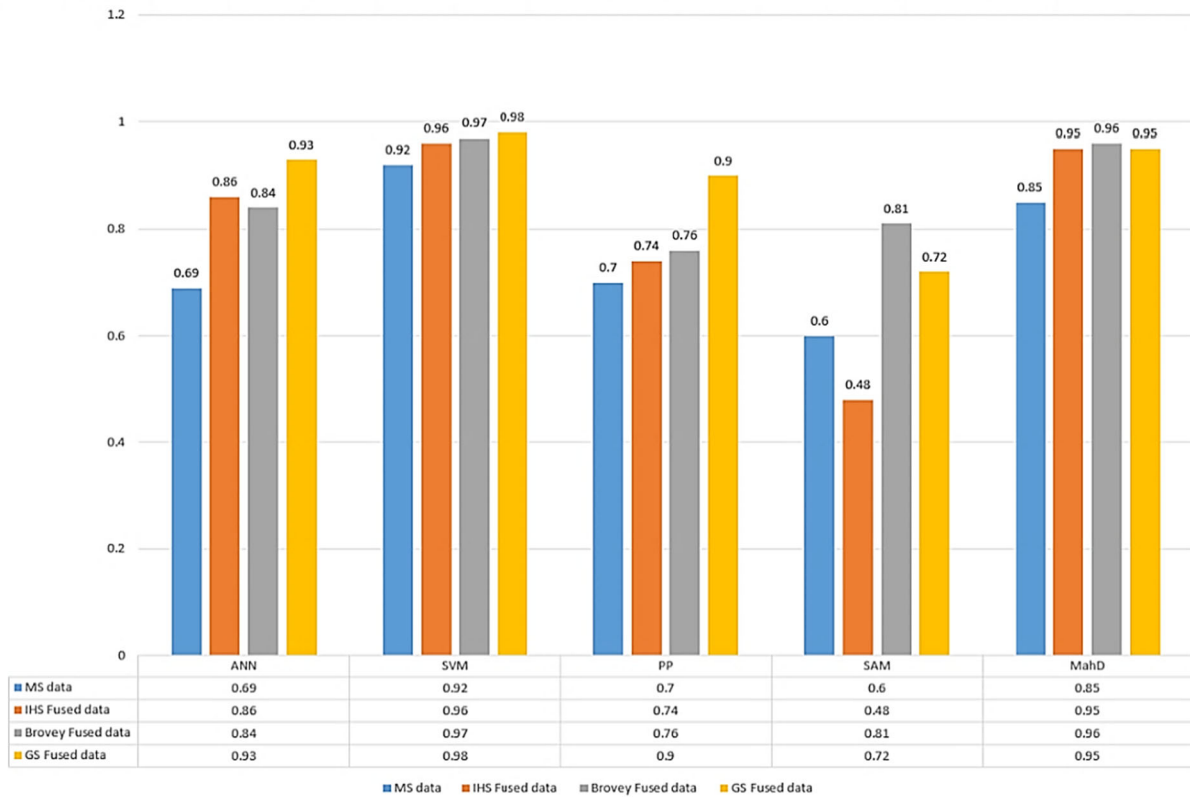


Fig. 12 Kappa coefficients of MS and fused data

Figure 12 indicates that the all-accurate assessment values were obtained for all the adopted approaches from each classified image of the MS data and the three spectral pan-sharpening fused images. The SVM method was provided the best performance when applied on data of MS Landsat and PAN when they integrating together using the GS pan-sharpening technique. The classification outputs reveal that the accuracy obtained from adopting the SVM approach provides the highest results, the overall accuracy of about (99.85%) with a kappa coefficient of about (0.98) from image classification. However, the SAM classification of the fused image using IHS spectral pan-sharpening method shows the lowest accuracy overall images classifications by representing an overall accuracy of (53.41%) with the kappa coefficient about (0.48). The research aims to investigate and find out the possibility of using the PAN data to improve the estimation accuracy of the LULC thematic map. Therefore, based on all the results of this study, it is found that the optimal methodology to obtain the highest results for generating the LULC

thematic map for Baghdad city is by performing image integration of MS and PAN data using GS spectral pan-sharpening method and classify with the SVM method. Figure 13 illustrates the LULC estimated map of Baghdad city, this thematic map has five different classes (urbanization area, vegetation area, water bodies, soil area and roads).

6 Conclusion

This study investigates and analysis the use of Landsat-8 OLI both of MS and PAN datasets in order to find the best and the best and the most accurate method for LULC estimating in Baghdad city, Iraq by performing a statistical comparison between many classification approaches (SVM, SAM, Mah, PP and ANN) were applied on MS images and other three pan-sharpening fused images by IHS, Brovey and GS methods. The refined producer was proposed for LULC mapping regarding to the obtained results. The results validation was conducted by applying the

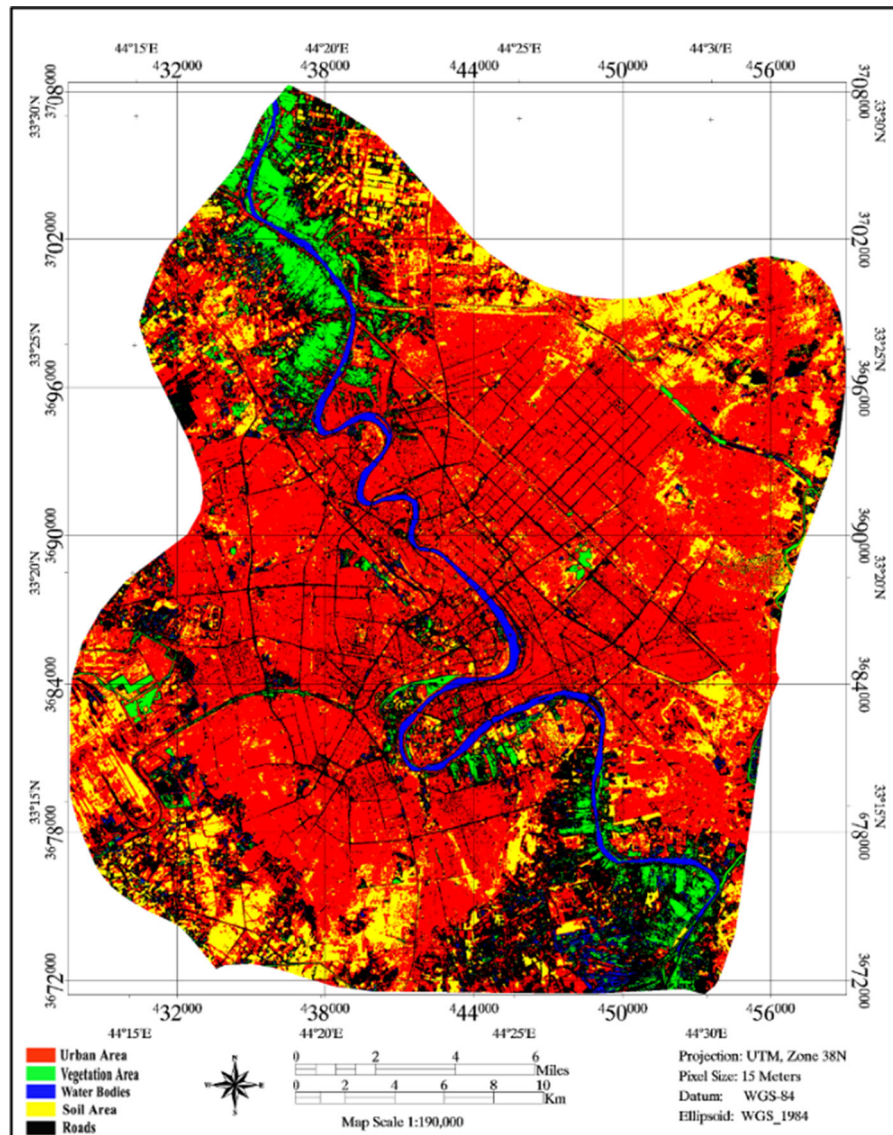


Fig. 13 Optimal LULC classification achieved by SVM method and GS sharpening fused image

confusion matrix. The obtained overall accuracy and kappa coefficient from applying the SVM classifier on the fused imagery by the GS spectral sharpening algorithm shows the highest accurate result over all other classifiers and the use of IHS and Brovey spectral sharpening fusion methods. The SVM approach achieves the highest results among all classification methods with different levels of image classifications; (1) with MS image, it is provided OA about 93.25% and kappa coefficient 0.92; (2) with classification of integrating IHS pan-sharpening spectral with MS image, SVM provides OA of 98.56% and

kappa coefficient about 0.96; (3) with classification of integrating Brovey sharpening spectral, it provides OA about 98.7% with a kappa coefficient of 0.97, and (4) with Gram–Schmidt Sharpening, SVM achieves OA about 99.85% with a kappa coefficient of 0.98. However, the SAM algorithm has the lowest accuracy compared to all other adopted methods, with OA 53.41% and the kappa coefficient about 0.48. Therefore, the outcome results confirm that the image fusion using the GS spectral algorithm and SVM classifier was determined as the best technique to estimate the thematic map of LULC for this study. In future work,

object-based approaches and methods should be examined and compared to the results of classification methods of pixel base. In addition, it should be trying to use satellite imagery has high spatial and spectral resolution; such as QuickBird, worldview-3, SPOT series, and IKONOS satellite systems.

Acknowledgements We would like to acknowledge the insightful contributions of the anonymous reviewers

Author Contributions “Conceptualization, HD and HAH.; methodology, HD and HAH.; software, HD and HAH.; validation, HD, HAH., ASM and NAA; investigation, HD and HAH.; data curation, HD and HAH.; writing—original draft preparation, HD, HAH., ASM and NAA.; visualization, NAA.; project administration, NAA; f All authors have read and agreed to the published version of the manuscript.”

Funding Open access funding provided by Lulea University of Technology.

Declarations

Conflict of interest The authors declare no conflict of interest.

Open Access This article is licensed under a Creative Commons Attribution 4.0 International License, which permits use, sharing, adaptation, distribution and reproduction in any medium or format, as long as you give appropriate credit to the original author(s) and the source, provide a link to the Creative Commons licence, and indicate if changes were made. The images or other third party material in this article are included in the article’s Creative Commons licence, unless indicated otherwise in a credit line to the material. If material is not included in the article’s Creative Commons licence and your intended use is not permitted by statutory regulation or exceeds the permitted use, you will need to obtain permission directly from the copyright holder. To view a copy of this licence, visit <http://creativecommons.org/licenses/by/4.0/>.

References

- Azarang A, Kehtarnavaz N (2020) Image fusion in remote sensing by multi-objective deep learning. *Int J Remote Sens* 41(24):9507–9524
- Aysar JA, Hayder D, Bashar H (2020) Interpolation and statistical analysis for evaluation of global earth gravity models based on GPS and orthometric heights in the middle of Iraq. *Iraqi J Sci* 61(7):1823–1830. <https://doi.org/10.24996/ijs.2020.61.7.31>
- Bello YI, Parviz GN (2013) Fusion of RADARSAT-2 and IKONOS images for land cover mapping: performance analysis. *Appl Remote Sens J* 3(1):18
- Bovolo F, Bruzzone L, Capobianco L, Garzelli A, Marchesi S (2010) Analysis of effect of pan-sharpening in change detection on VHR Images. *IEEE Trans Geosci Remote Sens Lett* 7(1):53–57. <https://doi.org/10.1109/LGRS.2009.2029248>
- Chasmer L, Hopkinson C, Veness T, Quinton W, Baltzer JA (2014) Decision-tree classification for low-lying complex land cover types within the zone of discontinuous permafrost. *Remote Sens Environ* 143:73–84. <https://doi.org/10.1016/j.rse.2013.12.016>
- Cavur M, Duzgun HS, Kemeç S, Demirkan DC (2019) Land use and land cover classification of Sentinel 2-A: St Petersburg case study. In: *ISPRS of the Photogrammetry, Remote Sensing & Spatial Information Sciences 2019*, vol XLII-1/W2, pp 13–16. <https://doi.org/10.5194/isprs-archives-XLII-1-W2-13-2019>
- Dibs H, Al-Janabi A, Gomes C (2017) Easy to use remote sensing and GIS analysis for landslide risk assessment. *J Univ Babylon Eng Sci* 26(1):42–54
- Dibs H (2018) Comparison of derived Indices and unsupervised classification for AL-Razaza Lake dehydration extent using multi-temporal satellite data and remote sensing analysis. *J Eng Appl Sci* 13(24):1–8
- Dibs H (2013) Feature extraction and based pixel classification for estimation the land cover thematic map using hyper-spectral data. *Int J Eng Res Appl* 3(3):686–693
- Dixon G, Leni C, Antonio C, Sofronio C, Sangjun I (2015) Land use characterization and change detection of a small mangrove area in Banacon island, Bohol, Philippines using a maximum likelihood classification method. *For Sci Technol* 11(4):97–205
- Elatawneh A, Kalaitzidis C, Petropoulos GP, Schneider T (2014) Evaluation of diverse classification approaches for land use/cover mapping in a Mediterranean region utilizing hyperion data. *Int J Digit Earth* 7(3):194–216. <https://doi.org/10.1080/17538947.2012.671378>
- Ghosh A, Sharma R, Joshi PK (2014) Random forest classification of urban landscape using landsat archive and ancillary data: combining seasonal maps with decision level fusion. *Appl Geogr* 48:31–41. <https://doi.org/10.1016/j.apgeog.2014.01.003>
- Hayder D, Suhad AH, Hasan SAK (2018) Extraction detailed buildings 3D model with using high resolution satellite imagery by remote sensing and GIS analysis; AL-Qqasim Green University A Case Study. *Int J Civ Eng Technol (IJCIET)* 9(7):1097–1108
- Hayder D, Shattri M, Noordin A, Biswajeet P (2015) Band-to-band registration model for near-equatorial Earth observation satellite images with the use of automatic control point extraction. *Int J Remote Sens* 36(8):2184–2200. <https://doi.org/10.1080/01431161.2015.1034891>
- Hayder D, Hashim H, Jawad KA, Nadhir A (2020) An optimal approach for land-use/land-cover mapping by integration and fusion of multispectral landsat OLI images: case study in Baghdad, Iraq. *Water Air Soil Pollut* 231(9):488. <https://doi.org/10.1007/s11270-020-04846-x>
- Hashim H, Hayder D, Abdulameer SD, Nadhir A (2020a) Monitoring and assessment of salinity and chemicals in agricultural lands by a remote sensing technique and soil moisture with chemical index models. *Geosciences (switzerland)* 10(207):1–20
- Hashim H, Hussain AJ, Hayder D, Hussain MH, Nadhir A (2020b) Evaluation of water quality parameters in marshes

- zone southern of Iraq based on remote sensing and GIS techniques. *Water Air Soil Pollut* 231(4):1–11
- Hayder D, Suhad A (2019) Detection wetland dehydration extent with multi-temporal remotely sensed data using remote sensing analysis and GIS techniques. *Int J Civ Eng Technol* 10(1):143–154
- Iounousse J, Er-Raki S, Motassadeq AE, Chehouani H (2015) Using an unsupervised approach of probabilistic neural network (PANN) for land use classification from multi-temporal satellite images. *Appl Soft Comput* 30:1–13. <https://doi.org/10.1016/j.asoc.2015.01.037>
- Jain S, Sachdeva M, Dubey P, Vijan A (2019) Multi-sensor image fusion using intensity hue saturation technique. In: International conference on advanced informatics for computing research. Springer, Singapore, pp 147–157
- Karar HF, Hussein S, Hayder D (2020) Spatial–temporal analysis of land use and land cover change detection using remote sensing and GIS techniques. *IOP Conf Ser Mater Sci Eng* 671(1):012046. <https://doi.org/10.1088/1757-899X/671/1/012046>
- Khatami R, Mountrakis G, Stehman SV (2016) A meta-analysis of remote sensing research on supervised pixel-based land-cover image classification processes: general guidelines for practitioners and future research. *Remote Sens Environ* 177:89–100
- Liu Q (2018) Sharpening the WBSI imagery of Tiangong-II: Gram–Schmidt and principal components transform in comparison. In: 2018 14th international conference on natural computation, fuzzy systems and knowledge discovery (ICNC-FSKD), IEEE, pp 511–518
- Li H, Jing L, Tang Y, Wang L (2018) An image fusion method based on image segmentation for high-resolution remotely-sensed imagery. *Remote Sens* 10(5):790
- Lu D, Li G, Moran E, Dutra L, Batistella M (2011) A comparison of multisensor integration methods for land cover classification in the Brazilian Amazon. *Geosci Remote Sens* 48(3):345–370. <https://doi.org/10.2747/1548-1603.48.3.345>
- Löw F, Conrad C, Michel U (2015) Decision fusion and non-parametric classifiers for land use mapping using multi-temporal rapideye data. *ISPRS J Photogramm Remote Sens* 108:191–204. <https://doi.org/10.1016/j.isprsjprs.2015.07.001>
- Li X, Li L, He MA (2017) Novel Pansharpening Algorithm for WorldView-2 Satellite Images. <http://www.ipcsit.com/131/004-ICIII2012-C0010>
- Li G, Lu D, Moran E, Dutra L, Batistella M (2012) A comparative analysis of ALOS PALSAR L-Band and RADARSAT-2 C-band data for land-cover classification in a tropical moist region. *ISPRS J Photogramm Remote Sens* 70:26–38. <https://doi.org/10.1016/j.isprsjprs.2012.03.010>
- Ma J, Ma Y, Li C (2019) Infrared and visible image fusion methods and applications: a survey. *Inf Fusion* 45:153–178
- Pushparaj J, Hegde AV (2017) Evaluation of pan-sharpening methods for spatial and spectral quality. *Appl Geom* 9(1):1–12
- Paidamwoyo M, Willard M, Naledzani M (2020) Comparison of image fusion techniques using satellite Pour l’Observation de la Terre (SPOT) 6 Satellite Imagery. *Appl Sci* 10:1881. <https://doi.org/10.3390/app10051881>
- Rwanga SS, Ndambuki JM (2017) Accuracy assessment of land use/land cover classification using remote sensing and GIS. *Int J Geosci* 8(04):611
- Sang H, Zhang J, Zhai L, Qiu C, Sun X (2014) Analysis of rapideye imagery for agricultural land cover and land use mapping. In: 2014 3rd international workshop on earth observation and remote sensing applications (EORS) 2014, Changsha. IEEE, pp 366–369
- Singh SK, Srivastava PK, Gupta M, Thakur JK, Mukherjee S (2014) Appraisal of land use/ land cover of mangrove forest ecosystem using support vector machine. *Environ Earth Sci* 71(5):2245–2255. <https://doi.org/10.1007/s12665-013-2628-0>
- Saha S, Bovolo F, Bruzzone L (2019) Unsupervised deep change vector analysis for multiple-change detection in VHR images. *IEEE Trans Geosci Remote Sens* 57(6):3677–3693
- Taubenböck H, Felbier A, Esch T, Roth A, Dech S (2012) Pixel-based classification algorithm for mapping urban footprints from radar data: a case study for RADARSAT-2. *Can J Remote Sens* 38(3):211–222. <https://doi.org/10.5589/m11-061>
- Xing Y, Wang M, Yang S, Jiao L (2018) Pan-sharpening via deep metric learning. *ISPRS J Photogramm Remote Sens* 145:165–183
- Yuan Q, Wei Y, Meng X, Shen H, Zhang L (2018) A multiscale and multidepth convolutional neural network for remote sensing imagery pan-sharpening. *IEEE J Sel Topics Appl Earth Observ Remote Sens* 11(3):978–989
- Yifang B, Alexander J (2013) Object-based fusion of multi-temporal multi-angle ENVISAT ASAR and HJ-1B multi-spectral. *IEEE Trans Geosci Remote Sens* 51(4):1998–2006
- Zhang C, Pan X, Li H, Gardiner A, Sargent I, Hare J, Atkinson PM (2018) A hybrid MLP-CNN classifier for very fine resolution remotely sensed image classification. *ISPRS J Photogramm Remote Sens* 140:133–144
- Zoleikani R, Zoj MJV, Mokhtarzadeh M (2017) Comparison of pixel and object oriented based classification of hyperspectral pansharpened images. *J Indian Soc Remote Sens* 45:25–33. <https://doi.org/10.1007/s12524-016-0573-6>
- Zhong J, Yang B, Huang G, Zhong F, Chen Z (2016) Remote sensing image fusion with convolutional neural network. *Sens Imaging* 17(1):1–16

Publisher’s Note Springer Nature remains neutral with regard to jurisdictional claims in published maps and institutional affiliations.